

## Supporting information

Mechanism and quantitative assessment of saturation transfer for water-based detection of the aliphatic protons in carbohydrate polymers

Yang Zhou, Peter C. M. van Zijl, Jiadi Xu, and Nirbhay N. Yadav

## Supporting Theory

### *The glycoNOE magnetization transfer model*

The glycoNOE magnetization transfer from an aliphatic proton to water is described by the following simplified two-step model:



where  $H_a$ ,  $H_e$  and  $H_w$  represent a glycogen aliphatic proton pool, a neighboring exchangeable (hydroxyl) proton pool and the free water proton pool, respectively.  $\sigma_{ae}$  and  $\sigma_{ea}$  are the “effective” NOE longitudinal cross-relaxation rates, and  $k_{ew}$  and  $k_{we}$  are the exchange rates of the neighboring hydroxyl and the water protons, respectively.

### *Numerical simulation*

According to the above three-pool model (M1), the  $x$ ,  $y$ ,  $z$ -magnetization evolutions of  $H_a$ ,  $H_e$  and  $H_w$  under the irradiation of a continuous radio frequency (RF) pulse can be described numerically by the following full set of modified Bloch equations (1) (ignoring  $J$ -coupling effects),

$$\frac{d}{dt} \mathbf{M} = \mathbf{R} \cdot \mathbf{M} \quad [S1]$$

where  $\mathbf{M}$  represents the magnetization column vector  $[U/2 \ A_x \ A_y \ A_z \ E_x \ E_y \ E_z \ W_x \ W_y \ W_z]$ , and

$$\mathbf{R} = \begin{bmatrix}
 0 & 0 & 0 & 0 & 0 & 0 & 0 & 0 & 0 & 0 \\
 0 & -\lambda_a & -\Omega_a & 0 & -\mu & 0 & 0 & 0 & 0 & 0 \\
 0 & \Omega_a & -\lambda_a & \omega_1 & 0 & -\mu & 0 & 0 & 0 & 0 \\
 2\Theta_a & 0 & -\omega_1 & -\rho_a & 0 & 0 & -\sigma_{ea} & 0 & 0 & 0 \\
 0 & -\mu & 0 & 0 & -\lambda_e - k_{ew} & -\Omega_e & 0 & k_{we} & 0 & 0 \\
 0 & 0 & -\mu & 0 & \Omega_e & -\lambda_e - k_{ew} & \omega_1 & 0 & k_{we} & 0 \\
 2\Theta_e & 0 & 0 & -\sigma_{ae} & 0 & -\omega_1 & -\rho_e - k_{ew} & 0 & 0 & k_{we} \\
 0 & 0 & 0 & 0 & k_{ew} & 0 & 0 & -\lambda_w - k_{we} & -\Omega_w & 0 \\
 0 & 0 & 0 & 0 & 0 & k_{ew} & 0 & \Omega_w & -\lambda_w - k_{we} & \omega_1 \\
 2\Theta_w & 0 & 0 & 0 & 0 & 0 & k_{ew} & 0 & -\omega_1 & -\rho_w - k_{we}
 \end{bmatrix} \quad [S2]$$

with,

$$\Theta_a = \rho_a A_{z,0} + \sigma_{ea} E_{z,0} \quad [S3]$$

$$\Theta_e = \rho_e E_{z,0} + \sigma_{ae} A_{z,0} \quad [S4]$$

$$\Theta_w = \rho_w W_{z,0} \quad [S5]$$

where  $\rho_a$ ,  $\rho_e$  and  $\rho_w$  are the longitudinal relaxation rates (without chemical exchange contributions) for glycogen aliphatic protons ( $H_a$ ), exchangeable protons ( $H_e$ ) and free water protons ( $H_w$ );  $\lambda_a$ ,  $\lambda_e$  and  $\lambda_w$  are the transverse relaxation rates (without chemical exchange contributions) for the three pools.  $\Omega_a$ ,  $\Omega_e$ ,  $\Omega_w$  are the chemical shift offsets of the three pools referenced to water;  $\omega_1$  is the radial frequency of the saturation field  $B_1$  ( $\omega_1 = \gamma B_1$ ).  $\mu$  is the transverse cross-relaxation rate,  $\sigma_{ae}$  and  $\sigma_{ea}$  are the longitudinal cross-relaxation rates. The time-dependent evolution of magnetization can be calculated numerically by solving Eq. S1

$$\mathbf{M} = \exp(-\mathbf{R}t) \quad [S6]$$

In the simulation program, the values (or ranges) of parameters (2) were set as shown in Table 1 in the main text. The Z-spectra were constructed by calculating the z-magnetization of water as a function of saturation offset.

### *Analytical calculation*

It is cumbersome to derive the exact analytical solutions of Eqs. S1-S5 due to their complexity. To gain some intuitive insight into the glycoNOE signal dependence, we derived the analytical solutions of z-magnetization in the steady-state scenario. From Eqs. S1 and S2, the z-magnetization evolutions of three pools under a continuous-wave (cw) field ( $\omega_1$ ) applied on  $H_a$ , are described by,

$$\frac{dA_z}{dt} = -\rho_a (A_z - A_{z,0}) - \sigma_{ea} (E_z - E_{z,0}) - \omega_1 A_y \quad [S7]$$

$$\frac{dE_z}{dt} = -\rho_e (E_z - E_{z,0}) - \sigma_{ae} (A_z - A_{z,0}) - k_{ew} E_z + k_{we} W_z \quad [S8]$$

$$\frac{dW_z}{dt} = -\rho_w (W_z - W_{z,0}) + k_{ew} E_z - k_{we} W_z \quad [S9]$$

From the proton chemical exchange equilibrium  $k_{we} [H_w] = k_{ew} [H_e]$  (where  $[H_w]$  and  $[H_e]$  are the populations of the two pools), it can be seen that  $-k_{ew} E_{z,0} + k_{we} W_{z,0} = 0$ , and Eqs. S8, S9 can also be written as,

$$\frac{dE_z}{dt} = -\rho_e (E_z - E_{z,0}) - \sigma_{ae} (A_z - A_{z,0}) - k_{ew} (E_z - E_{z,0}) + k_{we} (W_z - W_{z,0}) \quad [\text{S10}]$$

$$\frac{dW_z}{dt} = -\rho_w (W_z - W_{z,0}) + k_{ew} (E_z - E_{z,0}) - k_{we} (W_z - W_{z,0}) \quad [\text{S11}]$$

When only the glycogen proton  $H_a$  is saturated and a steady state is reached in the system,  $\frac{dE_z}{dt} =$

0, and  $\frac{dW_z}{dt} = 0$ :

$$-\rho_e (E_z - E_{z,0}) - \sigma_{ae} (A_z - A_{z,0}) - k_{ew} (E_z - E_{z,0}) + k_{we} (W_z - W_{z,0}) = 0 \quad [\text{S12}]$$

$$-\rho_w (W_z - W_{z,0}) + k_{ew} (E_z - E_{z,0}) - k_{we} (W_z - W_{z,0}) = 0 \quad [\text{S13}]$$

From Eq. S13,

$$E_z - E_{z,0} = \frac{\rho_w + k_{we}}{k_{ew}} (W_z - W_{z,0}) \quad [\text{S14}]$$

Apply Eq. S14 into Eq. S12,

$$\left[ k_{we} - (\rho_e + k_{ew}) \frac{\rho_w + k_{we}}{k_{ew}} \right] (W_z - W_{z,0}) - \sigma_{ae} (A_z - A_{z,0}) = 0 \quad [\text{S15}]$$

From Eq. S15,

$$\text{glycoNOE} \equiv \frac{(W_{z,0} - W_z)}{W_{z,0}} = \frac{-\sigma_{ae}}{(\rho_e + k_{ew}) \frac{\rho_w + k_{we}}{k_{ew}} - k_{we}} * \frac{A_{z,0} - A_z}{A_{z,0}} * \frac{A_{z,0}}{W_{z,0}} \quad [\text{S16}]$$

The term  $\alpha = \frac{A_{z,0} - A_z}{A_{z,0}}$  is the saturation efficiency at steady-state, with a value in the range of 0 to

1 depending on the  $B_1$  field strength applied on  $H_a$ , and the longitudinal relaxation rate. The enhancement factor “e” is,

$$e = \frac{-\sigma_{ae}}{(\rho_e + k_{ew}) \frac{\rho_w + k_{we}}{k_{ew}} - k_{we}} \quad [\text{S17}]$$

$f = \frac{A_{z,0}}{W_{z,0}}$ . For a solvent with 100% H<sub>2</sub>O,  $f = \frac{A_{z,0}}{W_{z,0}} = \frac{[H_a]}{[H_w]} = \frac{[H_e]}{[H_w]} = \frac{k_{we}}{k_{ew}}$ . Let's define the water proton fraction as P (P = 1 for H<sub>2</sub>O and 0.05 for 95% D<sub>2</sub>O). In the case of 95% D<sub>2</sub>O, 95% of the glycogen hydroxyl positions are taken by deuterons (OD) and only 5% are OH. During an experiment, the H<sub>a</sub> protons are continuously saturated but only the proton hydroxyl (OH) residues will efficiently couple to the H<sub>a</sub> protons and transfer the saturation to water and contributed to the detected proton signal (H<sub>w</sub>). Looking at 1 H<sub>a</sub>/H<sub>c</sub> pair, we have:  $[H_a]_{\text{effective}} = [H_e] = P * [\text{hydroxyl}]$  and  $[H_w] = P * 2 * [\text{water}]$ ; So the ratio  $[H_e] / [H_w]$  does not change with the enrichment. And  $f = \frac{A_{z,0}}{W_{z,0}} = \frac{[H_a]_{\text{effective}}}{[H_w]} = \frac{[H_e]}{[H_w]} = \frac{P * [\text{hydroxyl}]}{P * 2 * [\text{water}]}$ . So  $f$  also does not change with the proton enrichment.

Notice that any proton leaving the solvent will most likely replace a deuterium in glycogen. But it is indifferent whether this proton replaces a proton or deuterium, because it will end up next to an H<sub>a</sub> and then get saturated and go back to the solvent. Assuming approximately equal exchange rates for D and H, the same exchange rates can thus be used to describe the process, but  $[H_a]$  has to be replaced by  $[H_a]_{\text{effective}}$ . Assuming negligible transfer from D to H, the overall saturation effect on the proton signal detected would be the same. In agreement with this, we show that the glycoNOE signal intensity in D<sub>2</sub>O is about 3 fold of that in H<sub>2</sub>O (see Fig. 6 in the main text), with the glycoNOE difference being all due to water T<sub>1</sub> relaxation time difference in two solvent. After correcting water T<sub>1</sub> relaxation time, the glycoNOE intensity will be about the same in the two solvent.

Therefore, at steady-state,

$$\text{glycoNOE} = \alpha * e * f \quad [\text{S18}]$$

Notice the similarity with the analytical solution for the CEST effect at steady state (3-5).

Obtaining the analytical solution for  $\alpha$  without approximation would require solving the full sets of Eqs. S1-S6 analytically. For simplification, the evolution of  $H_a$  is assumed to be that of a single-spin system under  $\omega_1$ . That is,

$$\alpha = \frac{A_{z,0} - A_z}{A_{z,0}} \approx \frac{T_{1a}T_{2a}\omega_1^2}{1 + T_{1a}T_{2a}\omega_1^2 + (T_{2a}\Omega_a)^2} \quad [\text{S19}]$$

where  $T_{1a}$  and  $T_{2a}$  are the “effective” relaxation rates of  $H_a$  in a single-spin system, different from the terms  $\rho_a$  and  $\lambda_a$  in the three-pool model, Eq. S19 was deduced from the solution of steady-state Bloch equations under continuous wave on-resonance irradiation (6). Based on the fact that both the numerical simulation and experimental data analysis (see Figs. 3 and 4d in main text) using Eq. S19 describe the  $\alpha$  dependence well, this approximation appears to be valid for this spin system in glycogen.

For glycogen in  $\text{H}_2\text{O}$ , the chemical exchange rate is always much faster than the NOE relaxation rate (see Table S1), that is, assuming the slow tumbling limit,  $\rho_e \approx -\sigma_{ae}$ , to apply. Then

$$k_{ew} \gg -\sigma_{ae} \approx \rho_e \quad [\text{S20}]$$

and

$$1 + \rho_e/k_{ew} \approx 1 \quad [\text{S21}]$$

And (with  $f$  also equal to  $\frac{k_{we}}{k_{ew}}$ ),

$$\text{glycoNOE} = \alpha * \frac{-\sigma_{ae} * f}{\rho_w(1 + \rho_e/k_{ew}) + \rho_e * f} \approx \alpha * \frac{-\sigma_{ae} * f}{\rho_w + \rho_e * f} \quad [\text{S22}]$$

Let  $k_{aw} = -\sigma_{ae} \approx \rho_e$ ,

Eq. S22 can be rewritten as,

$$\text{glycoNOE} \approx \alpha * \frac{k_{aw} * f}{\rho_w + k_{aw} * f} \quad [\text{S23}]$$

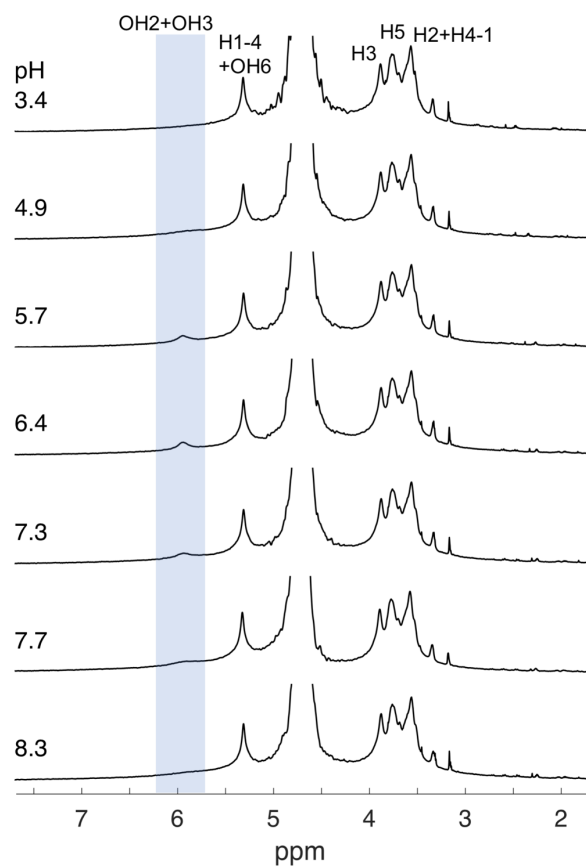
Eq. S23 is the analytical solution for a two-pool ( $H_a \xrightleftharpoons[k_{wa}]{k_{aw}} H_w$ ) CEST signal (7). Therefore, the

two-step model can be simplified to one step model. And Eq. S23 can be further simplified when

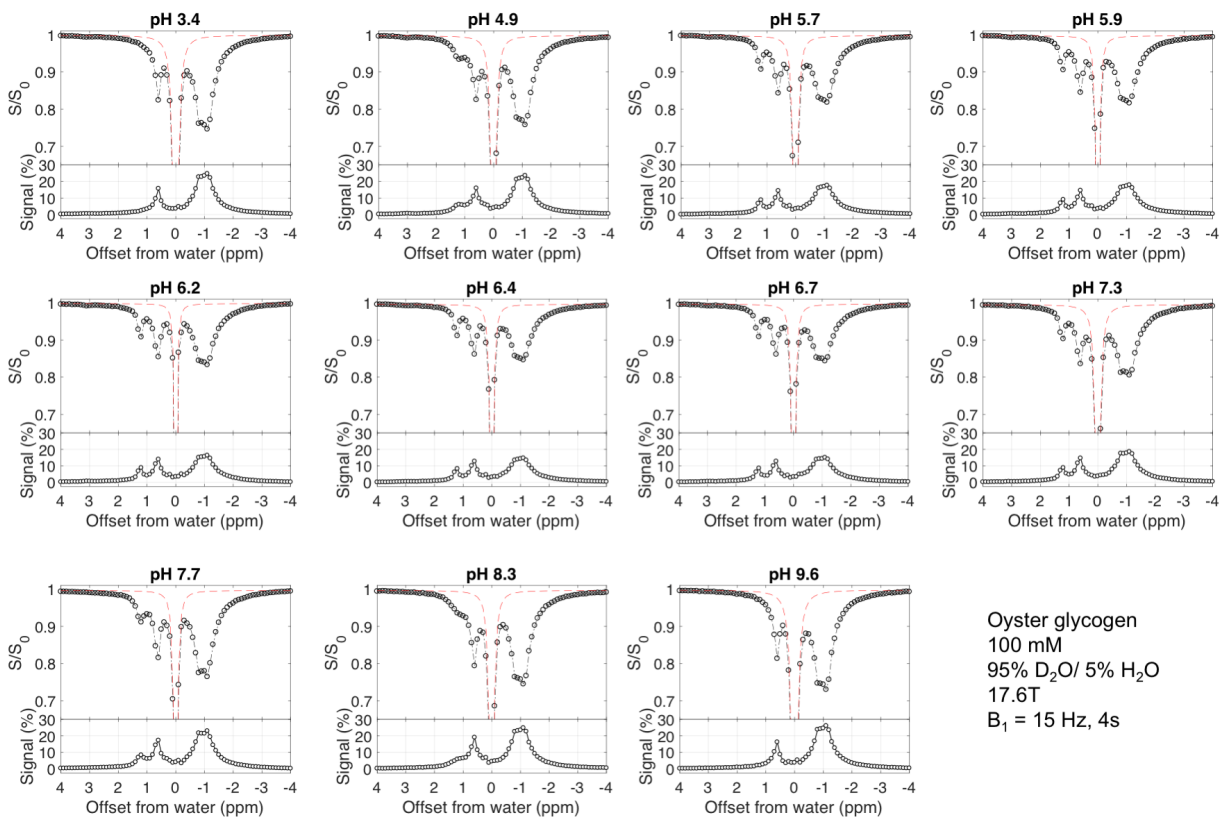
$\rho_w \gg k_{aw} * f$  (for instance, for 0.1M oyster glycogen in H<sub>2</sub>O,  $\rho_w \approx 0.36 \text{ s}^{-1}$ ,  $k_{aw} * f \approx 33 \text{ s}^{-1} *$

$\frac{0.1M}{110M} \approx 0.03 \text{ s}^{-1}$ ),

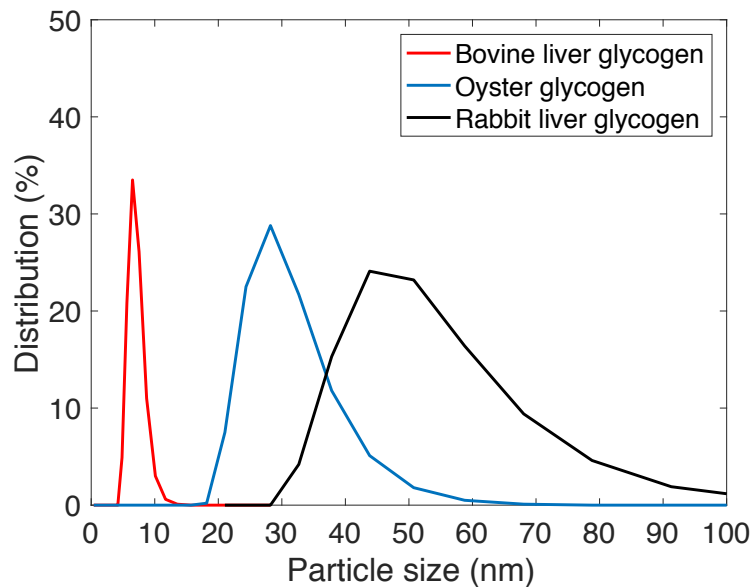
$$glycoNOE \approx \alpha * \frac{k_{aw} * f}{\rho_w} = -\alpha * \sigma_{ae} * T_{1w} * f \quad [S24]$$



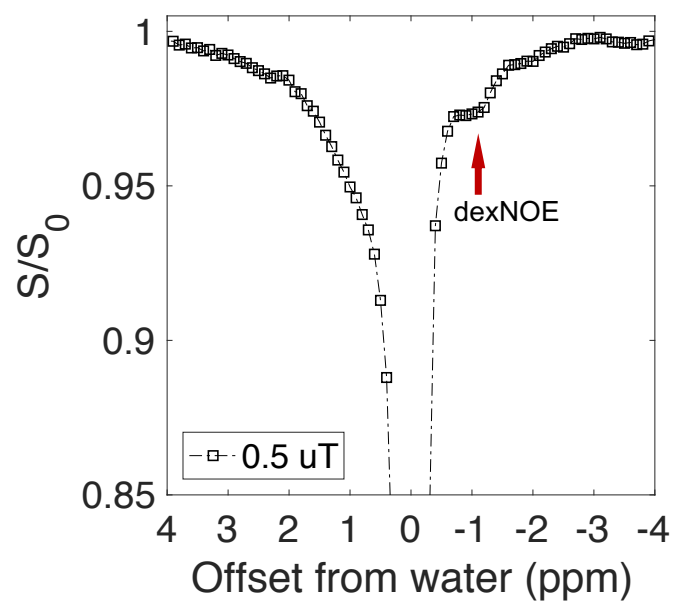
**Supporting Information Figure S1.** The visibility of glycogen hydroxyl protons in the proton NMR spectrum at different pH (100 mM in PBS buffer prepared with 95% D<sub>2</sub>O/5% H<sub>2</sub>O, 17.6T, 20°C).



**Supporting Information Figure S2.** The 17.6T Z-spectra for oyster glycogen (100 mM in PBS buffer prepared with 95% D<sub>2</sub>O/5% H<sub>2</sub>O, 20 °C) at different pH, using a continuous RF B<sub>1</sub> field, B<sub>1</sub> = 0.35 μT and t<sub>sat</sub> = 4s.



**Supporting Information Figure S3.** Particle size distribution of bovine liver glycogen, oyster glycogen and rabbit liver glycogen samples. Sizes of the commercial samples (Sigma) in PBS were measured using dynamic light scattering (DLS) based zetasizer (Zetasizer Nano ZS90, Malvern Instruments).



**Supporting Information Figure S4.** UTE-CEST scan (8) on dextran (~ 2000 kD) solution (200 mM glucose unit, pH 7.4, 20 °C) at 11.7 T.

**Supporting Information Table S1.** Estimated oyster glycogen (100 mM, 20 °C) hydroxyl exchange rates in D<sub>2</sub>O (95%) and H<sub>2</sub>O (95%) based on NMR linewidth analysis<sup>a</sup> and selective inversion recovery<sup>b</sup> analysis of the composite OH<sub>2</sub>+OH<sub>3</sub> peak (+1.2 ppm).

pH	$k_{ex}$ (s <sup>-1</sup> ) in D <sub>2</sub> O		$k_{ex}$ (s <sup>-1</sup> ) in H <sub>2</sub> O	
	Linewidth analysis <sup>a</sup>	Inversion recovery <sup>b</sup>	Linewidth analysis <sup>a</sup>	Inversion recovery <sup>b</sup>
4.5	NA	NA	675-857	NA
4.9	650-750	NA	402-583	290
5.7	60-170	70	245-426	350
5.9	70-170	110	214-395	300
6.2	0-110	50	352-533	470
6.4	50-160	90	349-530	500
6.7	40-150	90	760-942	550
7.3	190~300	330	NA	1500
7.7	700~810	NA	NA	NA

<sup>a</sup>The half-height linewidth ( $\nu_{1/2}$ ) depends on apparent T<sub>2</sub>:  $\nu_{1/2} = \frac{1}{\pi T_2} = \frac{(R_2^* + k_{ex})}{\pi}$ .  $R_2^*$  is the apparent transverse relaxation rate from non-chemical-exchange contributions.  $R_2^*$  is largely uncertain, but the lower boundaries can be estimated from H1-4 peak linewidth (at pH 9.6), and the upper boundary can be estimated from OH<sub>2,3</sub> peak width at pH 6.2 in D<sub>2</sub>O (267 Hz, assuming zero exchange rate). Therefore,  $R_2^*$  is estimated to be in the range of 119~267 s<sup>-1</sup> in D<sub>2</sub>O and 86~267 s<sup>-1</sup> in H<sub>2</sub>O. The hydroxyl exchange rates at different pH can be therefore estimated.

<sup>b</sup>The apparent longitudinal relaxation rate ( $R_1$ ) in selective inversion recovery experiments of OH<sub>2</sub>+OH<sub>3</sub> is:  $R_1 = \rho + k_{ex}$ .  $\rho$  is the longitudinal relaxation rate from non-chemical-exchange contributions.  $\rho$  values of hydroxyl protons were assumed to be similar to that of aliphatic proton H1-4, which were measured to be 33 s<sup>-1</sup> in H<sub>2</sub>O and 45 s<sup>-1</sup> in D<sub>2</sub>O (see main text Table. 2).

## References

1. Allard P, Helgstrand M, Härd T. A method for simulation of NOESY, ROESY, and off-resonance ROESY spectra. *Journal of Magnetic Resonance* 1997;129(1):19-29.
2. Zang LH, Laughlin MR, Rothman DL, Shulman RG. Carbon-13 NMR relaxation times of hepatic glycogen in vitro and in vivo. *Biochemistry* 1990;29(29):6815-6820.
3. Zhou J, Wilson DA, Sun PZ, Klaus JA, van Zijl PC. Quantitative description of proton exchange processes between water and endogenous and exogenous agents for WEX, CEST, and APT experiments. *Magnetic resonance in medicine* 2004;51(5):945-952.
4. Goffeney N, Bulte JW, Duyn J, Bryant LH, Van Zijl PC. Sensitive NMR detection of cationic-polymer-based gene delivery systems using saturation transfer via proton exchange. *Journal of the American Chemical Society* 2001;123(35):8628-8629.
5. Yadav NN, Xu J, Xu X, Liu G, McMahon MT, van Zijl PC. General Theory of CEST Image Acquisition and Post-Processing. *Chemical Exchange Saturation Transfer Imaging: Jenny Stanford Publishing; 2017. p 73-112.*
6. Bloch F. Nuclear induction. *Physical review* 1946;70(7-8):460.
7. van Zijl PC, Jones CK, Ren J, Malloy CR, Sherry AD. MRI detection of glycogen in vivo by using chemical exchange saturation transfer imaging (glycoCEST). *Proceedings of the National Academy of Sciences* 2007;104(11):4359-4364.
8. Chen L, Wei Z, Chan KW, Cai S, Liu G, Lu H, Wong PC, van Zijl PC, Li T, Xu J. Protein aggregation linked to Alzheimer's disease revealed by saturation transfer MRI. *NeuroImage* 2019;188:380-390.